water

MDPI

Article

Hydrochemistry of the Lhasa River, Tibetan Plateau: Spatiotemporal Variations of Major Ions Compositions and Controlling Factors Using Multivariate Statistical Approaches

Meizhuang Zhu [1,2], Xingxing Kuang [2,3,*], Yuqing Feng [2], Yinlei Hao [2], Qiule He [1,2], Hui Zhou [2], Jianxin Chen [2], Yiguang Zou [2] and Chunmiao Zheng [2]

1 School of Environment, Harbin Institute of Technology, Harbin 150090, China; 12149025@mail.sustech.edu.cn (M.Z.); 12049008@mail.sustech.edu.cn (Q.H.)
2 School of Environmental Science and Engineering, Southern University of Science and Technology, Shenzhen 518055, China; fengyq@sustech.edu.cn (Y.F.); haoyl@sustech.edu.cn (Y.H.); 11930476@mail.sustech.edu.cn (H.Z.); chenjx@mail.sustech.edu.cn (J.C.); 12032354@mail.sustech.edu.cn (Y.Z.); zhengcm@sustech.edu.cn (C.Z.)
3 Shenzhen Municipal Engineering Lab of Environmental IoT Technologies, School of Environmental Science and Engineering, Southern University of Science and Technology, Shenzhen 518055, China
* Correspondence: kuangxx@sustech.edu.cn

Abstract: Spatiotemporal variations of the hydrochemical major ions compositions and their controlling factors are essential features of a river basin. However, similar studies in the southern Tibetan Plateau are relatively limited. This study focuses on the chemical compositions of the dissolved loads in the Lhasa River (LR) in the southern Tibetan Plateau. Two sampling campaigns were conducted during the rainy and dry seasons across the LR basin to systematically investigate the spatiotemporal variations of water chemistry and sources of the dissolved loads. The results show that the river water possesses slight alkalinity with an average pH of 8.05 ± 0.04. Total dissolved solids (TDS) and oxidation-reduction potential (ORP) range widely from 39.8 mg/L to 582.6 mg/L with an average value of 165.6 ± 7.7 mg/L and from −9.4 mV to 295 mV with a mean value of 153.7 ± 6.9 mV, respectively. The major cations follow the decreasing order of Ca^{2+}, Mg^{2+}, Na^{+}, and K^{+} while HCO_3^{-}, SO_4^{2-}, Cl^{-}, and NO_3^{-} for anions. Ca^{2+} and Mg^{2+} account for 87.8% of the total cations, while HCO_3^{-} and SO_4^{2-} accounts for 93.9% of the total anions. All the major ions show higher concentrations in the dry season. NO_3^{-}, HCO_3^{-}, and Mg^{2+} show significant spatial variations due to the influence of basin lithology and anthropogenic activity. Multi-variables statistical analysis reveals that the mechanisms controlling the LR hydrochemistry are mainly carbonate weathering followed by silicate weathering. Geothermal springs and anthropogenic activities also play crucial roles in altering river water ions composition in the middle stream and downstream. The relatively high NO_3^{-} value (3 ± 0.2 mg/L) suggests water quality will be under the threat of pollution with the increase of anthropogenic activities.

Keywords: major ions; spatiotemporal variations; controlling factors; hydrochemistry; Lhasa River

Citation: Zhu, M.; Kuang, X.; Feng, Y.; Hao, Y.; He, Q.; Zhou, H.; Chen, J.; Zou, Y.; Zheng, C. Hydrochemistry of the Lhasa River, Tibetan Plateau: Spatiotemporal Variations of Major Ions Compositions and Controlling Factors Using Multivariate Statistical Approaches. *Water* **2021**, *13*, 3660. https://doi.org/10.3390/w13243660

Academic Editor: Elias Dimitriou

Received: 22 October 2021
Accepted: 14 December 2021
Published: 20 December 2021

1. Introduction

Rivers play an important role in industries and domestic water usage as well as irrigation [1]. Thus, the assessment of the water quality is a prerequisite for effective and reasonable water management. The river chemical compositions reflect the climate and environmental conditions where the river drains [2]. Previous studies suggested that the controlling factors of surface water chemistry are extremely complex and show spatiotemporal heterogeneity. Controlling factors include many natural processes, i.e., precipitation, parent rock weathering [3–5], evapo-crystallization process [6], tectonic movement, geographic and geomorphic conditions [3], and anthropogenic inputs (i.e., mining activities) [1,3], agricultural fertilizer [7,8], and city sewage [9]. Numerous studies

have been conducted to reveal the hydrochemistry signature and its controlling factors of the world's large river systems, including the Ganges-Brahmaputra [10,11], the Amazon River [12], the Mekong River [13], the Yangtze River [14], the Yellow River [4], and the Yarlung Tsangpo [3,5,13,15,16]. These studies not only identified sources of the dissolved loads but also calculated the weathering flux in the continent-river-ocean system [11].

The Tibetan Plateau, also named "Asia's water tower", possesses many glaciers [17,18] and is the source of many large rivers [19,20]. Due to climate warming, the glacier melting rate is accelerating [18,21], which will result in runoff rising [22–24] and alter the hydrochemistry of the rivers [25]. Therefore, the Tibetan Plateau and its adjacent region are gradually becoming a hotspot of river chemistry study [3,10,13,16].

The Lhasa River (LR) basin is situated in the southern Tibetan Plateau and is characterized by the densest population on the plateau [26], abundant geothermal springs [27–29], glacier distribution [30], and plentiful permafrost [31,32]. During the past forty years, the LR basin has been experiencing significant warming [33]. There are only a few studies have been carried out on hydrochemistry of the LR basin during the past years [34–36]. However, these studies were either investigated only in the summer [37,38] or only in the middle and lower reaches around city and towns. Systematic and comprehensive sampling campaigns are needed to accurately characterize the spatiotemporal variations of the LR hydrochemistry and reveal their controlling factors.

The objective of this study is to analyze the hydrochemistry of the LR during different seasons and investigate its controlling factors. The results of this study will help assess the water quality of the LR and identify the source of the dissolved loads in the LR during the rainy and dry seasons.

2. Study Area

The LR originated from the Nyenchen Tanglha Mountains, which is the largest tributary of the Yarlung Tsangpo (Figure 1). The LR basin is located at the southern Tibetan Plateau and extends from 90.1° E to 93.3° E and 29.3° N to 31.3° N with an area of 3.26×10^4 km^2. Elevation ranges from 3575 m to 7085 m with a mean altitude of 4500 m. Controlled by the South Asian monsoon, the LR basin is characterized by a temperature semiarid monsoon climate with perennial annual precipitation of 440 mm [26]. Precipitation displays huge spatiotemporal heterogeneity. The whole year can be divided into two seasons: dry season occurring from October to May of the following year; rainy season initiating from June to September when almost 90% of rainfall drop during this period [39,40]. The precipitation gradually decreases from northeast to southwest. The annual average air temperature is −1.7 to 9.7 °C [40].

Vegetation types display significant spatial differences with alpine meadows and subalpine steppes distributing in the up-and middle- stream whereas shrubs and forest in the lower reaches of the LR [38]. Soil types in the area are mainly alpine meadow soil, alpine desert soil, and sub-alpine steppe soil [40]. Geographic features are characterized by high mountains and valley plain [37]. Quaternary strata are widely distributed and composed of alluvial and diluvial deposits [36]. The lithology of the LR basin is dominated by the Mesozoic limestone and metamorphic sandstone and Himalayan granite [36] (Figure 1B).

The LR is fed by precipitation, glacier-snow meltwater, and groundwater [32]. In the upstream of the LR, the main anthropogenic activity is pasture husbandry [38]. The croplands and cities are mainly situated in the river valley of the lower reaches. There are abundant geothermal springs distributed within the LR basin along the Nyenchen Tanglha Mountains foothill [28,29] (Figure 1).

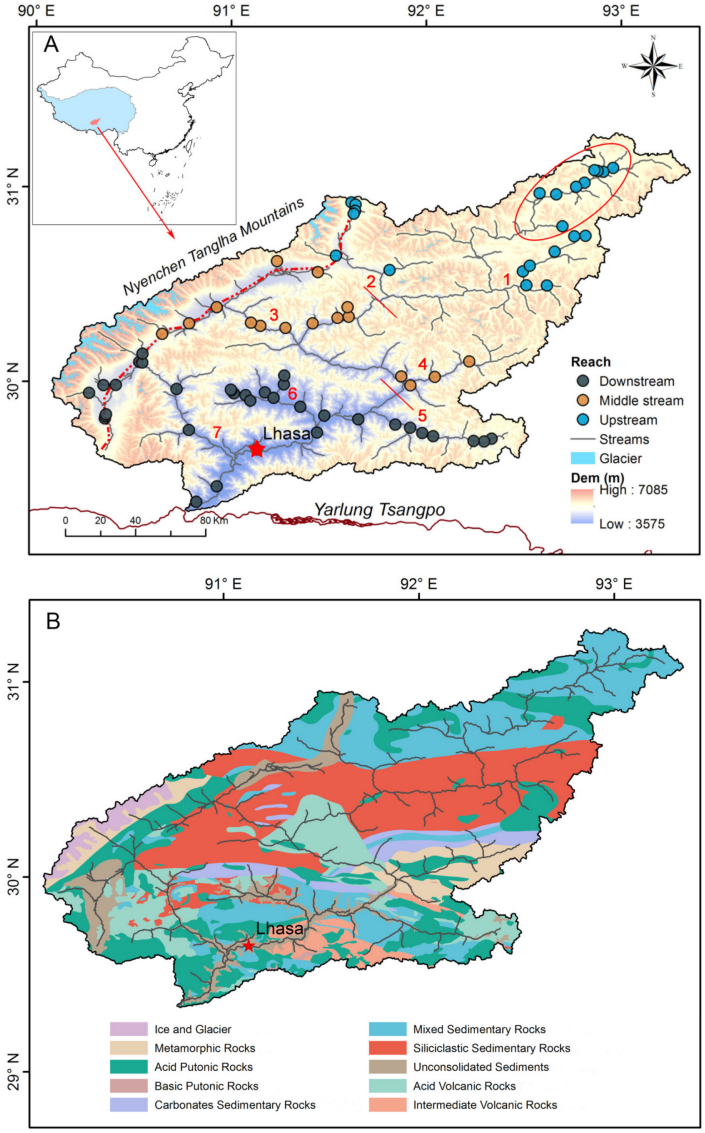

Figure 1. Location of the Lhasa River basin. (**A**) The sampling sites (marked by solid circles) during the rainy and dry seasons. The red short lines are nodes that divide the LR channel into the upstream, middle stream, and downstream, respectively. The red ellipse means the source area of the LR. The red numbers mean the tributaries of the Lhasa River, which are: 1 Maiqu; 2 Sangqu; 3 Wululongqu; 4 Xuerong Tsangpo; 5 Mozhuqu; 6 Pengboqu; 7 Duilongqu. The red dashed line is the geothermal water distribution zone. (**B**) Lithological map of the Lhasa River basin. The lithology data was obtained from the global lithological map (GLiM).

3. Materials and Methods

3.1. Sampling and Analyzing

Water samples of the LR basin were collected in August and November 2019, which belong to the rainy season and dry season, respectively. A total of 160 samples were collected at 80 sites during two seasons. Surface water samples include glacier meltwater, snow, tributaries, and mainstream. The basic hydrochemistry parameters were measured in situ with the portable multi-parameter meter (HANNA, Co., Laval, QC, Canada), including water temperature (Tw, ±0.15 °C), electrical conductivity (EC, ±1 μS/cm), dissolved oxygen (DO, ±1.5% to ±3%), pH (±0.02) and oxidation-reduction potentiometer (ORP, ±1.0 mV). All devices were calibrated with standard solutions before measurement. Samples were filtered with 0.45 μm Nuclepore filters (Advantec, Co., Tokyo, Japan) and injected into 50 mL polyethylene bottles for major anions (i.e., chloride (Cl^-), sulfate

(SO_4^{2-}) and nitrate (NO_3^-)) and cations (i.e., calcium (Ca^{2+}), magnesium (Mg^{2+}), sodium (Na^+), and potassium (K^+)) analysis. The snow and glacier ice samples were collected into plastic bags by wearing polyethylene gloves and then melted at room temperature and finally transferred into 50 mL polyethylene bottles. All of the sample bottles were sealed with parafilm and kept in a frozen environment until follow-up analysis.

Major ions (exclude HCO_3^-) were measured with ion chromatography (ICS-1100 Dionex. Co., Sunnyvale, CA, USA) and soluble silicate was determined by flow injection analysis catalytic spectrophotometric method (QuickChem® Method 31-114-27-1-D, Loveland, CO, USA) in School of Environmental Science and Engineering, Southern University of Science and Technology, China. The detection limits are 100 μg/L and 50 μg/L for major anions and cations, respectively. HCO_3^- was titrated with 0.16 N $H_2SO_4^{2-}$ cartridge (Hach Co., Loveland, CO, USA) in situ by the following method. First, 100 mL water sample was poured into a clean, 250-mL Erlenmeyer flask. Second, one phenolphthalein indicator powder pillow was poured into the sample and swirled to mix. Third, the sample was titrated with a sulfuric acid solution until the color changed from pink to colorless (pH ≈ 8.3). This value indicates the phenolphthalein alkalinity in the sample. Fourth, a bromcresol green-methyl red indicator was added and the titration continues until the color changed from green to red (pH ≈ 4.3 to 4.9). This value indicates the total alkalinity. Finally, hydroxide, carbonate, and bicarbonate alkalinity were calculated based on the alkalinity relationships. All of the samples possess the charge imbalance of less than 10% and most of them possess the charge imbalance of less than 5%.

3.2. Statistical Analysis

t-test and one-way analysis of variance (ANOVA) were conducted to compare the difference of major ions between rainy season and dry season, and among upstream, middle stream, and lower stream of the LR, respectively [41,42]. Multivariate statistical analysis is an effective method in analyzing the relationships of hydrochemistry parameters and has been widely used [43–46]. The Spearman correlation analysis was used to identify the relationships among hydrochemical variables [8,43]. Principle component analysis (PCA), a typical dimensionality reduction method used to extract the explanatory power of numerous variables [46–49], has been widely used to distinguish the origin of major ions [46,47,50]. The above multivariate statistical analysis was performed by the R program.

4. Results

4.1. General Hydrochemistry

Concentrations of major ions and basic water parameters of the LR and adjacent rivers are shown in Table 1. The mean value of pH is 8.1 indicating a slightly alkaline water environment. The T_w of LR varies from 0.1 to 19.7 °C during the sampling periods. TDS (TDS = $\sum(Ca^{2+} + Mg^{2+} + K^+ + Na^+ + HCO_3^- + SO_4^{2-} + Cl^- + NO_3^- + SiO_2$, in mg/L) ranges widely from 39.8 to 582.6 mg/L with a mean value of 165.6 ± 7.7 mg/L. The LR displays a relatively smaller TDS compared with surrounding rivers and a greater value than the global mean value of 120 mg/L [51] and the Yarlung Tsangpo 112 mg/L [13]. ORP reflects an oxidized environment with a mean value of 154 ± 7 mV. The smallest value of ORP (−9 mV) was shown at the lower reach suggesting the reducibility of tributary water.

Calcium is the most abundant cation ranging from 6.3 to 111.1 mg/L with a mean value of 27.5 ± 1.3 mg/L, followed by magnesium (5.0 ± 0.4 mg/L) and sodium (5.2 ± 0.6 mg/L). Potassium possesses the least proportion with merely mean content of 1.2 ± 0.1 mg/L. The relative proportions of cations can be presented in a ternary diagram (Figure 2). Almost all the points gathered towards the Ca^{2+} apex, which further illuminates calcium is the dominant cation accounting for 23 – 88.1% (68.5%) on an equivalent basis. Mg^{2+} and $Na^+ + K^+$ account for 5.1 – 48.9% (19.3%) and 2.6 – 66.7% (12.2%) of total cations, respectively.

Table 1. Mean value, minimum value (Min), maximum value (Max), and standard error (SE) of water chemistry data of the different reaches of the LR. Values of water chemistry data in the World Health Organization (WHO) and Chinese State Standard (CSS) for drinking water are also shown.

Sites	Statistics	pH	T_w	ORP	EC	TDS	Na^+	K^+	Ca^{2+}	Mg^{2+}	Cl^-	NO_3^-	SO_4^{2-}	HCO_3^-	SiO_2	Reference
Upstream	Mean	8.3	9.9	133	202.4	171.6	4.3	0.9	27.4	6.3	1.4	1.8	46.5	77.7	5.2	This study
	Min	7.3	0.5	−9.4	75	65.2	1	0.2	9.7	1.3	0.1	B.D.	13.1	22	0.3	
	Max	9.4	19	289	420	379.3	20.5	3.5	57.1	18.4	15.3	5.8	156.8	184.2	13.4	
	SE	0.1	1	15.1	14.3	12.4	0.6	0.1	2	0.7	0.4	0.2	4.6	6.8	0.4	
Middle stream	Mean	8.1	7.6	174.1	193.8	181.9	6	1.4	29.3	5.7	4.7	3.6	46.4	77.7	7.1	
	Min	6.8	0.1	53	58	43.2	1	0.3	7.8	0.3	0.1	B.D.	4.6	21	2.9	
	Max	8.6	17.6	267	553	500.7	52.3	8.4	87.7	27.2	44.3	8.3	205.2	230.6	20.3	
	SE	0.1	0.9	10.2	17.3	17.7	1.4	0.2	2.7	0.9	1.3	0.3	6.8	7	0.6	
Downstream	Mean	7.9	10.3	153.6	174.6	152.9	5.1	1.2	26.5	3.9	3.1	3.2	44.3	57.6	8	
	Min	5.5	0.3	19	35	39.8	0.8	0.1	6.3	0.8	0.1	B.D.	4.7	4.6	2.2	
	Max	8.7	19.7	295	664	582.6	64.3	6.1	111.1	22.5	46.8	10.7	410.4	146.4	36.3	
	SE	0.1	0.6	9.4	134.7	11	0.9	0.1	2.1	0.4	0.7	0.3	7.1	4	0.5	
Lhasa River	Mean	8.1	9.4	153.7	187	165.6	5.2	1.2	27.5	5	3.1	3	45.4	68.3	7	
	Min	5.5	0.1	−9.4	35	39.8	0.8	0.1	6.3	0.3	0.1	B.D.	4.6	4.6	0.3	
	Max	9.4	19.7	295	664	582.6	64.3	8.4	111.1	27.2	46.8	10.7	410.4	230.6	36.3	
	SE	0	0.4	6.6	8.4	7.7	0.6	0.1	1.3	0.4	0.5	0.2	4	3.3	0.3	
Yarlung Tsangpo	Mean	-	-	-	-	112	3	1	21	4	5	0	27	47	4	[13]
Mekong River	Mean	-	-	-	-	302	12	1	49	14	14	0	69	138	4	[13]
Source of the Yangtze River	Mean	8	-	-	-	778	157.7	5.5	53.4	22.9	233.7	1.3	114.9	188.5 [a]	-	[16]
Gandaki, Nepal	Mean	8.3	-	-	530	269	12.4	3.5	39.7	13.9	16	1.8	49.4	130.2	7.2	[8]
Global River	Mean	8	-	-	-	120	6.3	2.3	15	4.1	7.8	1	11.2	58.4	16.4	[51,52]
CSS	Mean	6.5−9.5	-	-	-	1000	200	-	-	-	250	50	250	-	-	[53]
WHO	Mean	6-8.5	-	-	-	1000	200	100	100	50	250	50	250	600	-	[54]

Note. B.D. means below detection limit; a means concentration of $HCO_3^- + CO_3^{2-}$; units for major ions concentration are in mg/L and EC in μs/cm. TDS = ∑ ($Ca^{2+} + Mg^{2+} + K^+ + Na^+ + HCO_3^- + SO_4^{2-} + Cl^- + NO_3^- + SiO_2$).

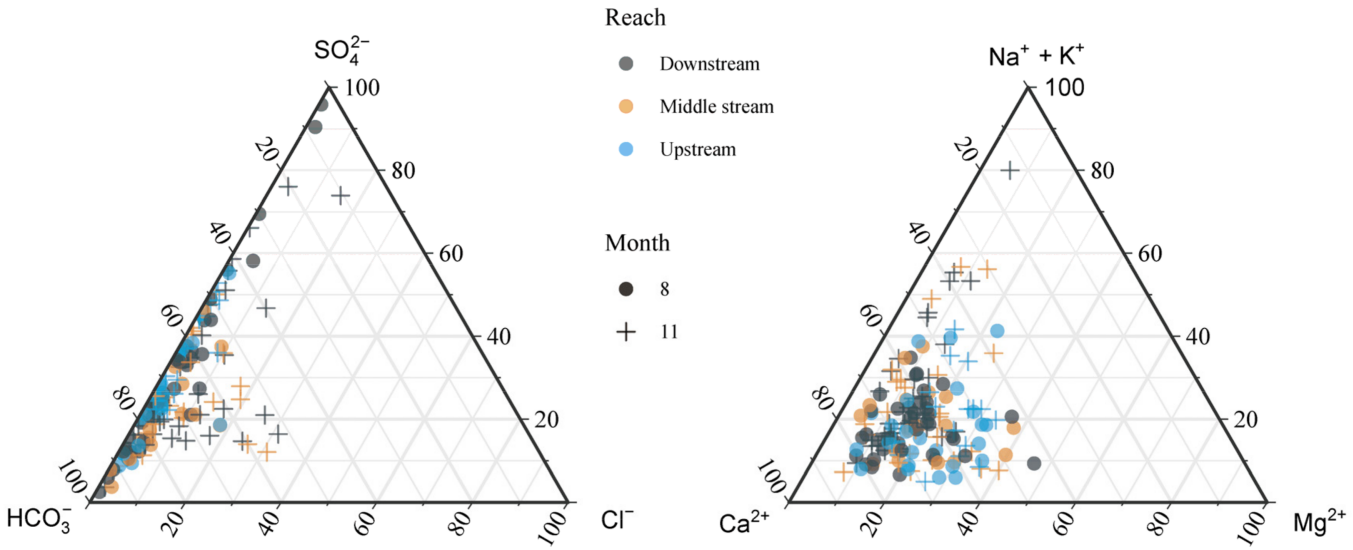

Figure 2. Ternary diagram of water samples in the LR during the rainy season and the dry season.

Bicarbonate and sulfate are the dominant anions with mean concentrations of 68.3 ± 3.3 mg/L and 45.4 ± 4.0 mg/L, respectively. Chloride displays a mean value of 3.1 ± 0.5 mg/L with the largest value (46.8 mg/L) shown in the downstream, which is affected by the surrounding geothermal springs [28]. The relatively high nitrate concentrations (3.0 ± 0.2 mg/L) are almost three times the global average value (1 mg/L, [51,52]). In the anion ternary diagram, all the sampling points distribute along the HCO_3^- axis. SO_4^{2-} and HCO_3^- together account for 72.3 – 99.4% (93.9% on average) of total anions on an equivalent basis, implying the major anions are SO_4^{2-} and HCO_3^-.

The water chemistry data of the LR is comparable to the other rivers derived from the Tibetan Plateau, indicating the LR water is relatively pristine. The LR possesses a relatively lower TDS compared with other rivers originated from the Tibetan Plateau (Table 1) whereas greater TDS than the global river mean value (120 mg/L, [51,52]). What is noteworthy is that NO_3^- of the LR is the highest among the surrounding rivers as well as the global mean value of 1 mg/L [51,52].

Surface waters in the LR basin show low mineralization (Tables 1 and 2). The mean values of all the chemical parameters are within the range in values of water chemistry data in the Chinese State Standard (CSS) [53] and World Health Organization (WHO) [54] for drinking water (Table 1). There is one sample from downstream with SO_4^{2-} exceeding the maximum limit, which should be caused by geothermal springs inputs.

4.2. Seasonal Variations of Hydrochemistry

In the rainy season, the mean value of surface water temperature is 13.7 ± 0.3 °C while it is only 5.2 ± 0.5 °C during the dry season. The ORP values reflect oxidized environments for water in both sampling seasons, with a mean value of 92 ± 4 mV in the rainy season and increased up to 215 ± 8 mV in the dry season. TDS displays considerable variations from 39.8 to 582.6 mg/L with a mean value of 138.7 ± 9.0 mg/L for the rainy season and from 47.3 to 557.4 mg/L with an average value of 192.5 ± 11.8 mg/L for the dry season, respectively. These findings are in accordance with the results around the Himalaya Mountains regions [8,55]. The seasonal variation of TDS results from precipitation and meltwater dilution [8].

Table 2. Arithmetic means standard error (Se), minimum and maximum values of water chemistry values of the LR major tributaries.

Tributaries	Statistics	Tw	pH	EC	ORP	Na^+	K^+	Ca^{2+}	Mg^{2+}	Cl^-	NO_3^-	SO_4^{2-}	HCO_3^-	TDS
Duilong Qu	Mean	7.6	8.1	158.9	102.1	8.3	1.5	21.5	2.8	5.6	3.7	35.4	52.1	141.5
	SE	1.1	0.1	14.8	7.4	2.6	0.2	1.5	0.4	2.1	0.4	5.8	5.6	14.5
	Min	0.3	7.3	59	19	1	0.7	7.8	0.3	0.3	0.5	5.3	7.3	43.2
	Max	18.8	8.7	379	160	64.3	6.1	40.5	7.9	46.8	9.5	111.6	144	391
Mai Qu	Mean	9.4	8.3	215.2	150.6	3.8	0.9	29.8	8.3	1.4	1.9	51.9	85.6	188.7
	Se	1.8	0.1	20.9	26.3	0.8	0.1	3.4	1.3	0.5	0.3	5.4	12.5	19.7
	Min	0.5	7.9	92	4.7	1	0.4	10.6	2.9	0.2	0.8	17.1	31.5	75
	Max	18	9.4	320	275	11.2	2.1	55.1	15.1	6	3.6	95.2	163.5	319.7
Mozhu Qu	Mean	8.2	7.5	122.3	190.4	2.5	0.7	19.9	2.8	0.8	2.2	42.1	31.2	108.4
	Se	0.5	0.2	18.8	20.8	0.4	0.1	3.7	0.4	0.3	0.2	10.5	5.2	15.9
	Min	4.3	5.5	35	83.4	0.8	0.1	6.3	1.7	0.1	0.3	10.5	4.6	39.8
	Max	11.4	8.4	325	295	7.6	1.2	56.6	8.4	5.1	4	177.1	98.7	255.1
Pengbo Qu	Mean	14.3	8.3	208.4	138.6	3.8	1.1	34.8	4.1	3.1	4.1	25.7	95.9	180.2
	Se	0.6	0.1	16.1	22.5	0.6	0.2	3.5	0.6	1	0.7	4.1	7.4	14.7
	Min	9.7	7.6	137	60.3	1.7	0.4	19.2	1.5	0.4	B.D.	4.7	46.4	109.7
	Max	19.7	8.6	354	281	11.2	3.0	66.4	10.6	15.1	9.4	68.6	146.4	327.2
Sang Qu	Mean	6.2	8.2	300.7	156.4	8.5	1.7	45	7.6	8.4	3.3	78.7	109.7	271.9
	Se	1.4	0.1	30.9	14.3	2.1	0.3	4.5	1.8	3.1	0.4	13.7	9.0	26.6
	Min	0.4	7.9	131	90.5	2.1	0.3	19.2	1.3	0.3	1.1	23.6	52.5	114.8
	Max	14.3	8.5	553	236	31	4.4	87.7	27.2	44.3	6	205.2	165.9	470.6
Source area	Mean	9.8	8.3	163.2	137.2	3.9	0.7	21.4	5.4	0.7	1	42.8	57.4	137.5
	Se	1.6	0.1	18.6	24.4	0.4	0.1	2.8	0.9	0.1	0.2	7.2	7.8	17.2
	Min	0.6	7.3	75	−9.4	1.4	0.2	9.7	1.7	0.1	B.D.	13.1	22	65.2
	Max	19	9.4	365	289	7.4	1.2	57.1	18.4	1.5	2.6	156.8	133	379.3
Wululong Qu	Mean	9.7	7.8	161.2	162.1	7.4	1.7	20.9	5.4	3	3.3	29.4	73.3	151.3
	Se	1.5	0.1	24.3	16.8	3.1	0.5	3	1.4	1.2	0.4	6.9	14.0	27.9
	Min	0.1	6.8	55	53	1	0.2	8.8	0.3	0.2	0.6	4.6	21.5	46.8
	Max	17.6	8.6	420	263	52.3	8.4	54	15.7	16.9	5.8	98.3	230.6	500.7
Xuerong Qu	Mean	8.9	7.9	150.9	179.7	1.9	0.7	23.8	4.3	0.7	1.6	40.9	52.6	131.3
	Se	1.1	0.2	9.9	25.3	0.3	0.1	1.8	0.5	0.3	0.4	3.4	6	9.9
	Min	4.3	7	109.0	96.5	1.3	0.6	18.3	2.5	0.1	B.D.	27.3	35.5	94.3
	Max	12.2	8.4	188.0	267	3.6	1	32.9	6.5	2.5	3	54.9	83	172.1

Note. B.D. means below detection limit; units for major ions concentration and TDS are in mg/L.

Ca^{2+} is the most abundant cation in both sampling periods and the mean value of the dry season is 1.45 times higher than that of the rainy season (Figure 3). K^+ shows the lowest value of 0.9 ± 0.1 mg/L and 1.4 ± 0.1 mg/L for the rainy and dry seasons, respectively. Concentrations of cations follow the decreasing order of Ca^{2+} > Mg^{2+} >Na^+ > K^+ during both sampling periods. Concentrations of anions follow the decreasing order of HCO_3^- > SO_4^{2-} > NO_3^- > Cl^- in the rainy season while change to HCO_3^- > SO_4^{2-} > Cl^- > NO_3^- in the dry season.

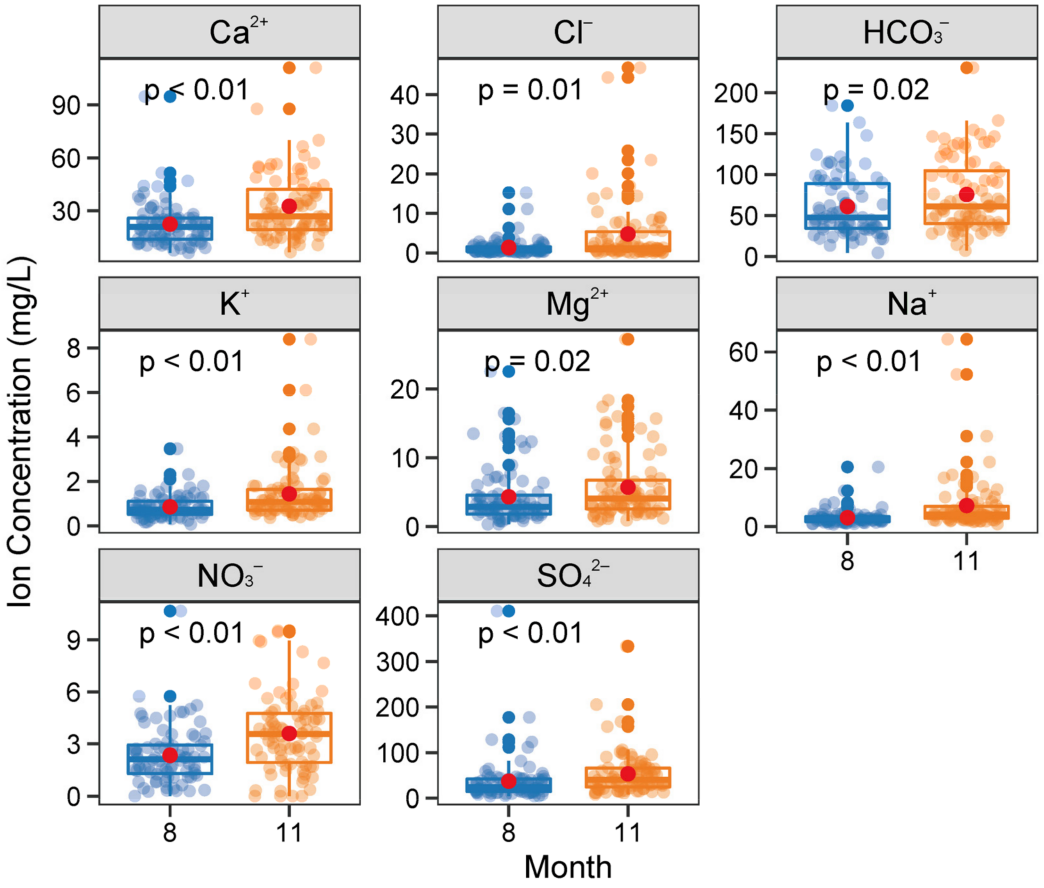

Figure 3. Boxplot of the major ions concentrations (in mg/L) during the rainy season and the dry season in the LR. Red circles are mean values. The significances of the major ions between different seasons are shown as *p* value.

It is worth noting that NO_3^- is an important hydrochemistry parameter that illustrates the interference of anthropogenic activities on streams. The concentrations of NO_3^- range from 0.02 to 10.7 mg/L and 0.02 to 9.7 mg/L with mean values of 2.7 ± 1.7 mg/L and 3.4 ± 2.3 mg/L for the rainy season and the dry season, respectively, and display significant temporal variations.

The T-test results show that all the major cations and anions show a significant temporal difference with $p < 0.05$ (Figure 3). It can be concluded that concentrations of major ions in the dry season are generally much higher than those of the rainy season, which may be caused by the integrated dilution effects of heavy precipitation and large amounts of glacier meltwater [8].

4.3. Spatial Distribution of Major Ions

Across the LR basin, the mean pH was found to be alkaline with the highest pH (9.4) noted from the upstream and the lowest pH (5.5) found in the Mozhu Qu (Table 2). Water samples from the middle stream possess higher TDS than those of upstream and downstream (Table 1). However, the highest (582.6 mg/L) and lowest TDS (39.8 mg/L)

values are from the downstream. Several samples collected adjacent to the Nyenchen Tanglha Mountains show significantly lower TDS, which are affected by the dilution effect of the glacier meltwater.

One-way ANOVA analysis indicates that HCO_3^-, Mg^{2+}, and NO_3^- show significant spatial variations with $p < 0.05$ among different reaches while other ions show no significant spatial variations with $p > 0.05$ (Figure 4). The concentration of K^+ is the lowest among the cations and its distribution is relatively even across the LR basin except for the largest value found in Wululong Qu (8.4 mg/L). Na^+ and K^+ display extremely high concentrations upstream of Sangqu, Wululongqu, and Duilongqu (Table 2), which is belonging to the geothermal springs belt [3]. Ca^{2+} and HCO_3^- are the predominant cation and anion, respectively, and unevenly distributed across the basin and display relatively higher values in the Mai Qu, Pengbo Qu, and Sang Qu. Mg^{2+}, as the second dominant cation, shows a relatively higher concentration in the middle and upper LR reaches. SO_4^{2-} shows the largest mean concentration in Sangqu River and the upper reaches of the LR. Cl^- displays high concentration along the geothermal springs belt but shows relatively low concentrations in the LR source region, Mozhu Qu, and Xuerong Tsangpo. The concentration of NO_3^- is unevenly distributed in the whole basin. The concentration of NO_3^- is much lower in upstream owing to the limited human activities. The concentration of NO_3^- gradually increases from upstream to downstream (Table 1). It should be noted that the mean value of NO_3^- is especially high in sites around cities and towns, which can be attributed to agricultural fertilizer usage and domestic wastewater discharge [38]. The elevated NO_3^- concentrations will threaten drinking water safety.

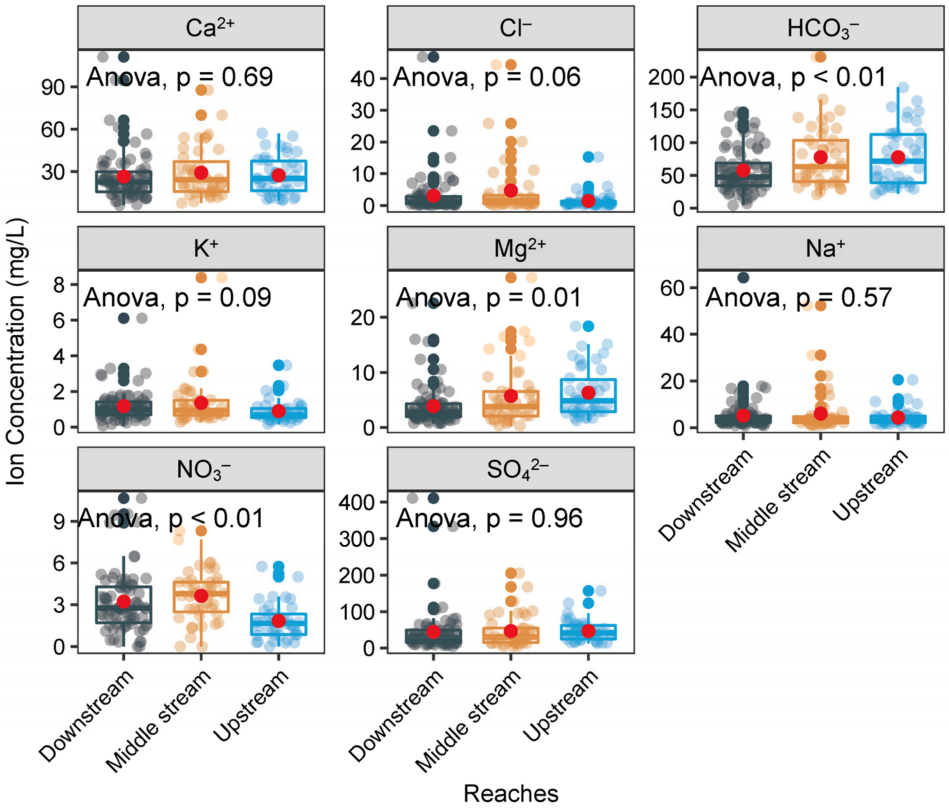

Figure 4. Boxplot of the concentrations of the major ions (in mg/L) for different reaches of the LR. One-way ANOVA analysis results for different ions are also shown in *p* values.

5. Discussion

5.1. Mechanisms Controlling the Major-Ion Chemistry

The major sources of dissolved loads can be classified into atmospheric input, parent rock weathering, and anthropogenic inputs [6]. The surface water samples collected from

both seasons are characterized by the medium TDS (165.6 ± 7.7 mg/L) and low ratios of $Na^+/(Na^+ + Ca^{2+})$ and $Cl^-/(Cl^- + HCO_3^-)$ (<0.5), which demonstrate the controlling role of rock weathering (Table 3). Chemical weathering of different lithologies yield complicated dissolved ions. For instance, carbonates (calcite and dolomite) weathering produce Ca^{2+}, Mg^{2+}, and HCO_3^-; silicates (albite, K-feldspar, Ca-plagioclase, and Olivine) weathering generates Na^+, K^+, Ca^{2+}, Mg^{2+}, Si, and HCO_3^-, and evaporates dissolution (halite and gypsum) are mainly the sources of Ca^{2+}, Mg^{2+}, Na^+, K^+, Cl^-, and SO_4^{2-} [10]. Thus, mixing diagrams of Na-normalized ions molar ratios (meq) have been used to display various end-member mixing [8,42,51]. Most of the samples collected from both seasons cluster towards the carbonates end-member, which implies the dominant role of carbonate (calcite and dolomite) weathering (Figure 5). Meanwhile, there are still some samples collected from the middle stream and downstream during the dry season gathering towards silicates and geothermal springs end-members, suggesting the origins of ions from silicate weathering and geothermal springs discharge.

Table 3. Ionic ratio (Mean ± Se) of the surface water during the rainy season and dry season in the different reaches of the LR (meq/L).

Variables	Rainy Season			Dry Season		
	Upstream	Middle Stream	Downstream	Upstream	Middle Stream	Downstream
HCO_3^-/Ca^{2+}	1.02 ± 0.05	1.06 ± 0.1	0.82 ± 0.05	0.79 ± 0.05	0.82 ± 0.04	0.78 ± 0.06
$(HCO_3^- + SO_4^{2-})/Ca^{2+}$	1.66 ± 0.05	1.58 ± 0.12	1.48 ± 0.05	1.65 ± 0.05	1.46 ± 0.06	1.4 ± 0.07
$(HCO_3^- + SO_4^{2-})/(Ca^{2+} + Mg^{2+})$	1.22 ± 0.02	1.18 ± 0.04	1.16 ± 0.03	1.16 ± 0.03	1.12 ± 0.03	1.14 ±0.05
$(HCO_3^- + SO_4^{2-})/(Ca^{2+} + Mg^{2+} + Na^+)$	1.11 ± 0.02	1.07 ± 0.04	1.06 ± 0.03	1.04 ± 0.03	0.98 ± 0.02	0.95 ± 0.02
$HCO_3^-/(HCO_3^- + SO_4^{2})^-$	0.62 ± 0.03	0.67 ± 0.04	0.56 ± 0.04	0.48 ± 0.03	0.57 ± 0.03	0.56 ± 0.03
$(Ca^{2+} + Mg^{2+})/TZ^+$	0.9 ± 0.01	0.89 ± 0.01	0.9 ± 0.01	0.88 ± 0.02	0.87 ± 0.02	0.84 ± 0.02
$(HCO_3^- + SO_4^{2-})/TZ^-$	0.97 ± 0.01	0.93 ± 0.01	0.95 ± 0.01	0.97 ± 0.0	0.92 ± 0.01	0.91 ± 0.01
Na^+/Cl^-	8.52 ± 1.33	3.72 ± 0.76	5.95 ± 0.54	10.48 ± 1.84	5.09 ± 0.96	6.78 ± 1.45
$Si/(Na^+ + K^+)$	0.73 ± 0.16	0.76 ± 0.07	0.92 ± 0.07	0.37 ± 0.06	0.52 ± 0.06	0.63 ± 0.04
Ca^{2+}/SO_4^{2-}	1.88 ± 0.17	2.75 ± 0.53	2.41 ± 0.4	1.33 ± 0.17	1.93 ± 0.22	2.39 ± 0.47
$(Ca^{2+} + Mg^{2+})/(Na^+ + K^+)$	13.04 ± 1.62	10.61 ± 1.37	10.86 ± 0.89	11.08 ± 2.07	11.09 ± 1.5	7.76 ± 0.7
$Na^+/(Na^+ + Ca^{2+})$ [a]	0.12 ± 0.02	0.11 ± 0.01	0.11 ± 0.01	0.14 ± 0.02	0.14 ± 0.02	0.17 ± 0.02
$Cl^-/(Cl^- + HCO_3^-)$ [a]	0.03 ± 0.01	0.06 ± 0.01	0.04 ± 0.01	0.03 ± 0.01	0.08 ± 0.02	0.1 ± 0.02

Note. Values expressed as mean ± Se, all ratios derived from meq concentrations and [a] ratios from mmol/L concentrations. Total dissolved cations: $TZ^+ = Na^+ + K^+ + 2 \times Mg^{2+} + 2 \times Ca^{2+}$ and total dissolved anions: $TZ^- = Cl^- + NO_3^- + 2 \times SO_4^{2-} + HCO_3^-$.

Ionic ratios can also further illustrate the origin of major ions yielded by chemical weathering (Table 3). Generally, carbonates are susceptible to weathering and can alter easily the hydrochemistry even though few carbonate rocks are presented in the bedrock [3,56]. The high equivalent ratios of $(Ca^{2+} + Mg^{2+})/(Na^+ + K^+)$ (7.8 ± 0.7 to 13 ± 1.6) and $(Ca^{2+} + Mg^{2+})/TZ^+$ (0.8 to 0.9 ± 0.01) also illustrate the dominant role of carbonates (calcite and dolomite) weathering on the LR water chemistry.

The equal ratios of Na^+ and Cl^- reflect Na^+ originates from the halite dissolution [57]. However, the concentration of Na^+ (in meq/L) is much higher than the concentration of Cl^- (Figure 6A and Table 3). The scatter plot of Cl^- and Na^+ exhibit that most samples lie above the 1:1 line, which implies the additional inputs, such as weathering of silicates and ion exchange [37] as well as geothermal springs input [3,28]. The excess Na^+ can be balanced by Si (Figure 6B). It can be seen that most of the samples lie on the 1:1 line, suggesting that Na^+ mainly originates from silicate weathering. There are still several points that lie above the 1:1 line, which may imply the additional Na^+ originates from geothermal springs input.

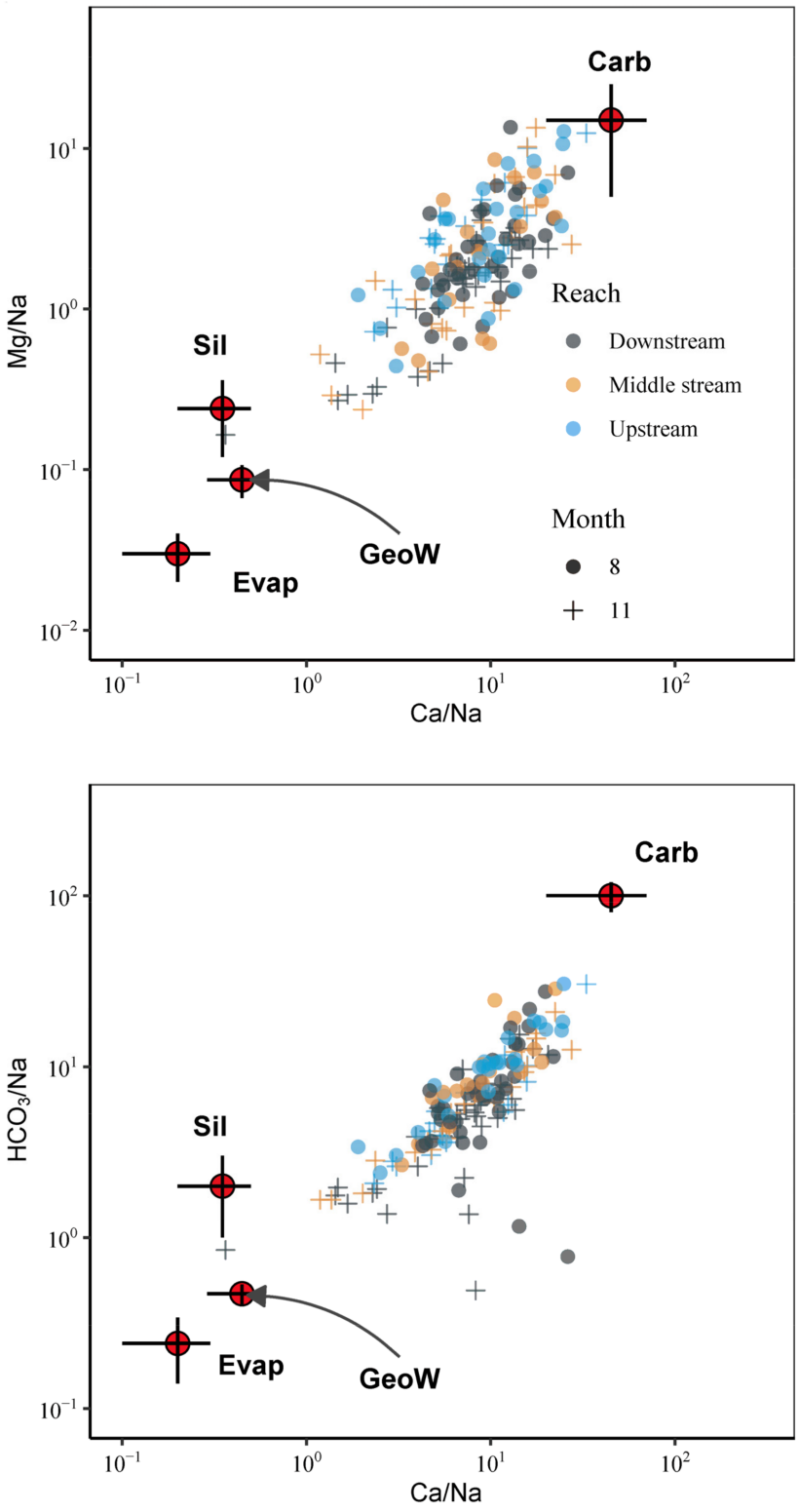

Figure 5. Mixing plot of Na-normalized ions molar ratios of the LR during rainy and dry seasons. End-members of evaporates (Evap), silicates (Sil), and carbonates (Carb) are attained from Gaillardet et al. [51]. End-member of geothermal water (GeoW) was obtained from Guo et al. [28,29].

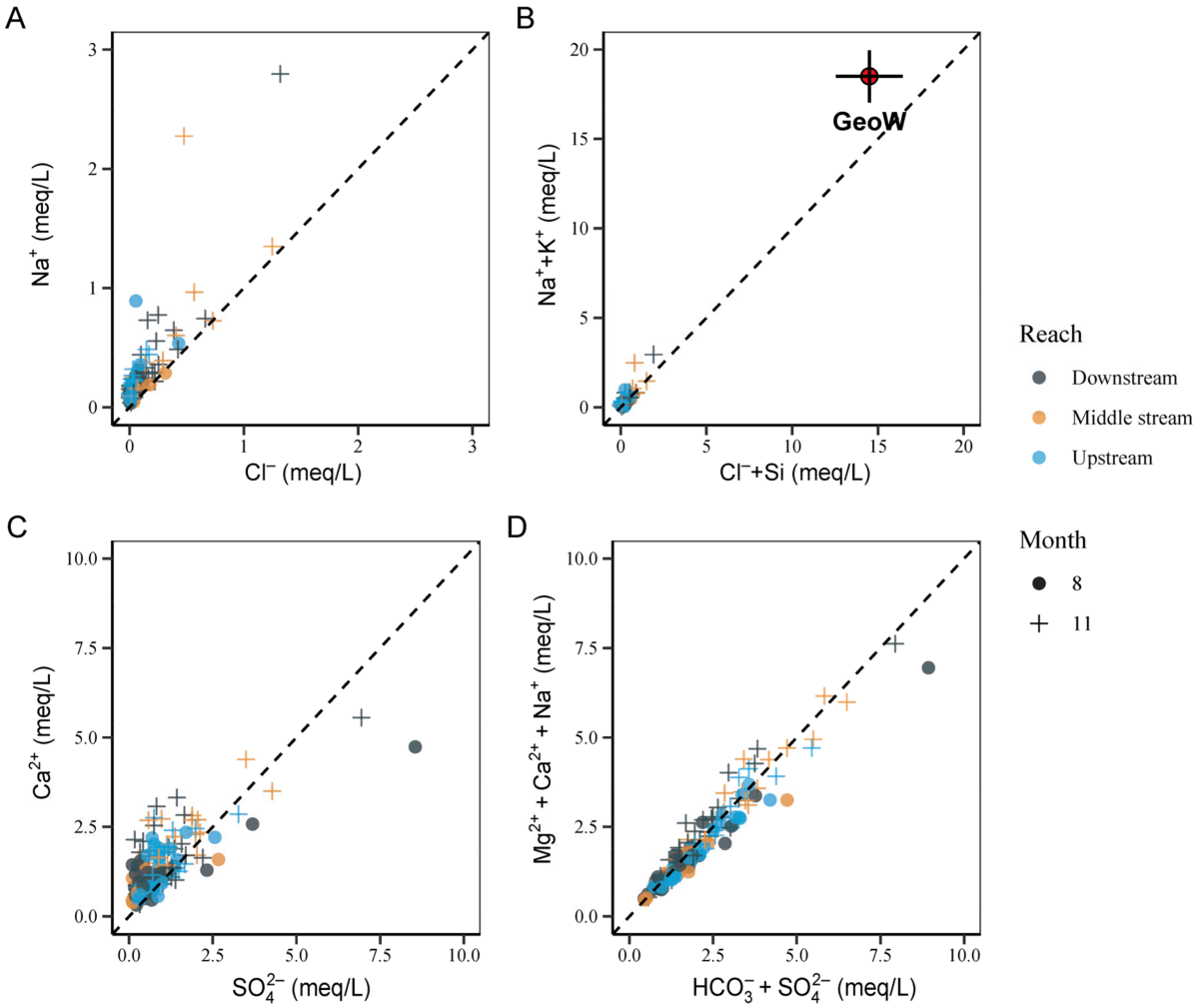

Figure 6. Cross-plot of major ions of the LR (in meq/L). (**A**) Na^+ vs. Cl^-: most of the samples lie above the 1:1 line, implying additional Na^+ sources except for halite dissolution; (**B**) $Na^+ + K^+$ vs. $Cl^- + Si$: most of the samples lie on the 1:1 line, suggesting excess Na^+ originated from silicate weathering; (**C**) Ca^{2+} vs. SO_4^{2-}: most of the samples lie above the 1:1 line, implying sulfate dissolution is limited; (**D**) $Mg^{2+} + Ca^{2+} + Na^+$ vs. $HCO_3^- + SO_4^{2-}$: almost all of the samples lie on the 1:1 line, implying the dominant role of carbonate weathering and the limited role of silicate weathering on the LR hydrochemistry. The dashed line in the figures represents lines with a slope of 1. End-member of geothermal water (GeoW) was obtained from Guo et al. [28,29].

$HCO_3^-/(HCO_3^- + SO_4^{2-})$ ratio (C-ratio) is an important indicator of proton source required for carbonate weathering [8]. If the C-ratio is less than 0.5, the coupled reaction of the sulfide oxidation and carbonate weathering are illuminated. When the C-ratio is close to 1, the carbonation reaction of atmospheric CO_2 is the dominant proton source [8]. The equivalent ratio of $HCO_3^-/(HCO_3^- + SO_4^{2-})$ is >0.5 for the whole LR basin during the rainy season and for the middle stream and downstream during the dry season, which indicates that the proton is originated from atmospheric CO_2. Whereas the proton of the upstream during the dry season is sulfide oxidation for the low equivalent ratio of $HCO_3^-/(HCO_3^- + SO_4^{2-})$ (0.48 ± 0.03). According to the lithological map (Figure 1B), the lithology of the sampling sites in upstream is mixed sedimentary rocks. The equivalent ratio of Ca^{2+}/SO_4^{2-} is greater than 1 (Figure 6C) further confirming that CO_2 dissolution is the major proton source.

The equivalent ratios of $(HCO_3^- + SO_4^{2-})/(Ca^{2+} + Mg^{2+} + Na^+)$ from different reaches are close to 1, which implies the dominant role of carbonate weathering and the limited role of silicate weathering on the LR hydrochemistry (Figure 6D). The hydrochemical characteristics of groundwater in the LR are characterized by moderate TDS and the major ions

originated from the weathered carbonates and silicate [36]. There are intensive hydraulic connections between groundwater and LR water and they are mutually transformed [58].

Overall, the mechanisms controlling the major ions chemistry display spatial variations. In the upstream, the major ions composition is dominated by carbonate weathering. While in the middle stream and downstream, besides lithology, anthropogenic activities and geothermal springs water input also play important roles in major ions chemistry.

The major ions of the LR and the rivers draining the Himalaya Mountains are both originated from chemical weathering. Carbonate weathering plays the dominant role in river hydrochemistry [56,59,60]. Previous studies have demonstrated that the rivers draining the Himalaya Mountains exhibit higher chemical weathering rates than the rivers originated from the Tibetan Plateau [3,55]. This can be attributed to heavy monsoon precipitation and rapid tectonic uplift along the Himalaya Mountains whereas low precipitation and cold environment on the Tibetan Plateau [3,10].

5.2. Multivariate Statistical Methods

The correlation matrix of water chemistry indices was used to investigate the dependency of one hydrochemistry parameter on the other. The correlations of geographical factors, water quality indices, and major ions concentrations are presented in Figure 7. The results indicate strong positive correlations between EC and TDS, Ca^{2+}, Mg^{2+}, HCO_3^-, and SO_4^{2-}. The positive correlations among Ca^{2+}, Mg^{2+}, and HCO_3^- in both sampling seasons suggest the contribution of the carbonates weathering to these ions. Ca^{2+}, Mg^{2+}, and SO_4^{2-} show positive correlations that illustrate probably the dissolution of gypsum or carbonate dissolution caused by sulfide oxidation [61]. However, Cl^- is not significantly correlated with SO_4^{2-} in the rainy and dry seasons (Figure 7), which implies that the dominant origins of SO_4^{2-} is from pyrite oxidation [3]. The source of SO_4^{2-} for the rivers draining the Himalaya Mountain is also originated from sulfide oxidation [3,10].

The significant positive correlations among Cl^-, Na^+, K^+, and SiO_2 during both sampling seasons imply the same source of these ions, possibly from the effect of weathering of silicate and geothermal springs inputs. Furthermore, elevation is strongly negatively associated with NO_3^- since anthropogenic activities are mainly carried out in the low elevation regions, which further suggests the effect of anthropogenic activities on the ion composition of water.

PCA was used to further reduce the dimensionality of the hydrochemical dataset containing considerable interrelated variables while retaining the variation shown in the dataset [46]. Four principal components (PCs) with eigenvalue > 1 were extracted explaining 70% of the total variance (Table 4 and Figure 8). PC1 has strong loadings on HCO_3^-, SO_4^{2-}, Ca^{2+}, Mg^{2+}, TDS, and EC accounting for 34.88–36.44% of the total variance, which indicates carbonate weathering is the dominant origin of these ions. PC2 explains 18.33–24.49% of the total variance with strong loadings of Na^+, Cl^-, SiO_2, and K^+, which suggest the mixing contribution of silicate weathering and geothermal springs [3]. PC3 is the factor of topography and climate with strong loadings of Elevation (Ele) and T_w, which explain 10.83–13.09% of the total variance. PC4 explains only 8.25–8.89% of the variance with strong loadings of NO_3^-, which can be attributed to the effect of anthropogenic activities. In general, the dominant source of ions is the parent rock weathering, followed by the geothermal springs' inputs and monsoon climate, as well as anthropogenic activity.

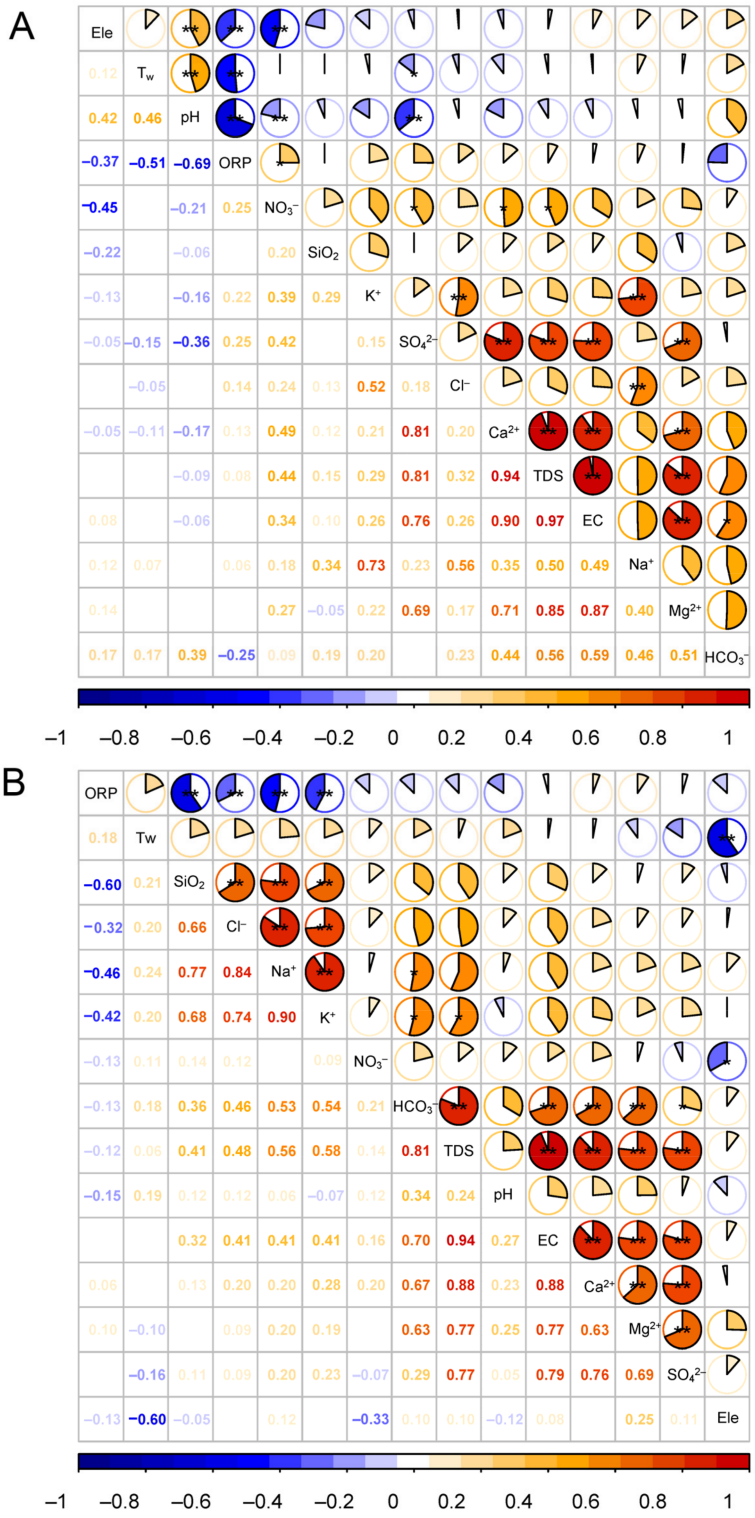

Figure 7. Heatmap of correlation coefficients among different hydrochemistry parameters in the rainy season (**A**) and the dry season (**B**). The pie charts area indicates the strength of the correlation. Blue and red colors mean positive and negative correlation coefficients, respectively. Meanwhile, * and ** mean significant levels with $p < 0.05$ and $p < 0.01$, respectively.

Table 4. Results of the principal component analysis on the first four rotated PCs during the rainy season and the dry season.

	Rainy Season				Dry Season			
	PC1	**PC2**	**PC3**	**PC4**	**PC1**	**PC2**	**PC3**	**PC4**
Elevation (ele)	0.08	0.08	0.29	**−0.81**	0.13	0.06	**−0.82**	−0.26
T_w	−0.04	−0.04	**0.74**	0.14	−0.03	0.20	**0.87**	0.07
TDS	**0.96**	0.25	0.03	0.09	**0.91**	0.40	0.00	0.10
pH	−0.10	−0.01	**0.83**	−0.26	0.21	−0.01	0.04	0.74
Cl	0.13	**0.75**	−0.11	−0.01	0.17	**0.85**	0.11	0.02
SiO_2	−0.04	0.40	0.15	0.52	0.05	**0.86**	0.02	0.18
ORP	0.05	0.13	**−0.83**	0.19	0.19	**−0.61**	0.44	−0.41
EC	**0.95**	0.23	0.06	0.01	**0.92**	0.25	0.00	0.13
NO_3^-	0.38	0.14	−0.10	**0.72**	0.05	0.06	0.23	**0.65**
SO_4^{2-}	**0.85**	−0.04	−0.32	0.10	**0.85**	0.01	−0.11	−0.15
HCO_3^-	0.46	0.40	0.53	−0.07	**0.67**	0.42	0.06	0.28
Na^+	0.30	**0.87**	0.07	−0.01	0.22	**0.94**	0.03	−0.05
K^+	0.10	**0.83**	−0.12	0.24	0.26	**0.89**	0.09	−0.11
Ca^{2+}	**0.93**	0.10	−0.06	0.17	**0.91**	0.05	0.09	0.16
Mg^{2+}	**0.89**	0.15	0.06	−0.11	**0.87**	−0.01	−0.16	0.08
Eigenvalue	5.42	2.75	1.96	1.24	5.9	2.86	1.87	1.14
Explained variance %	36.11	18.33	13.09	8.25	39.33	19.1	12.48	7.63
Cumulative variance %	36.11	54.44	67.53	75.78	39.33	58.43	70.91	78.54

Note: The bold fonts indicate the strong loadings.

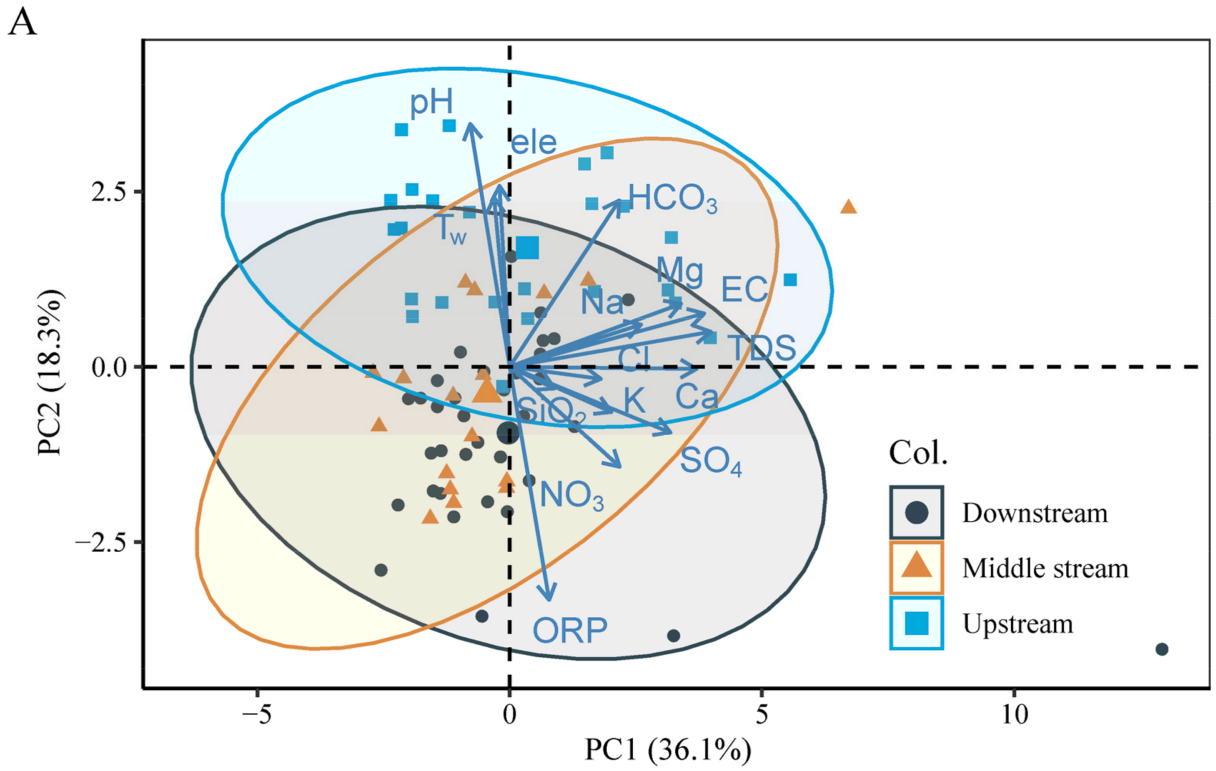

Figure 8. *Cont.*

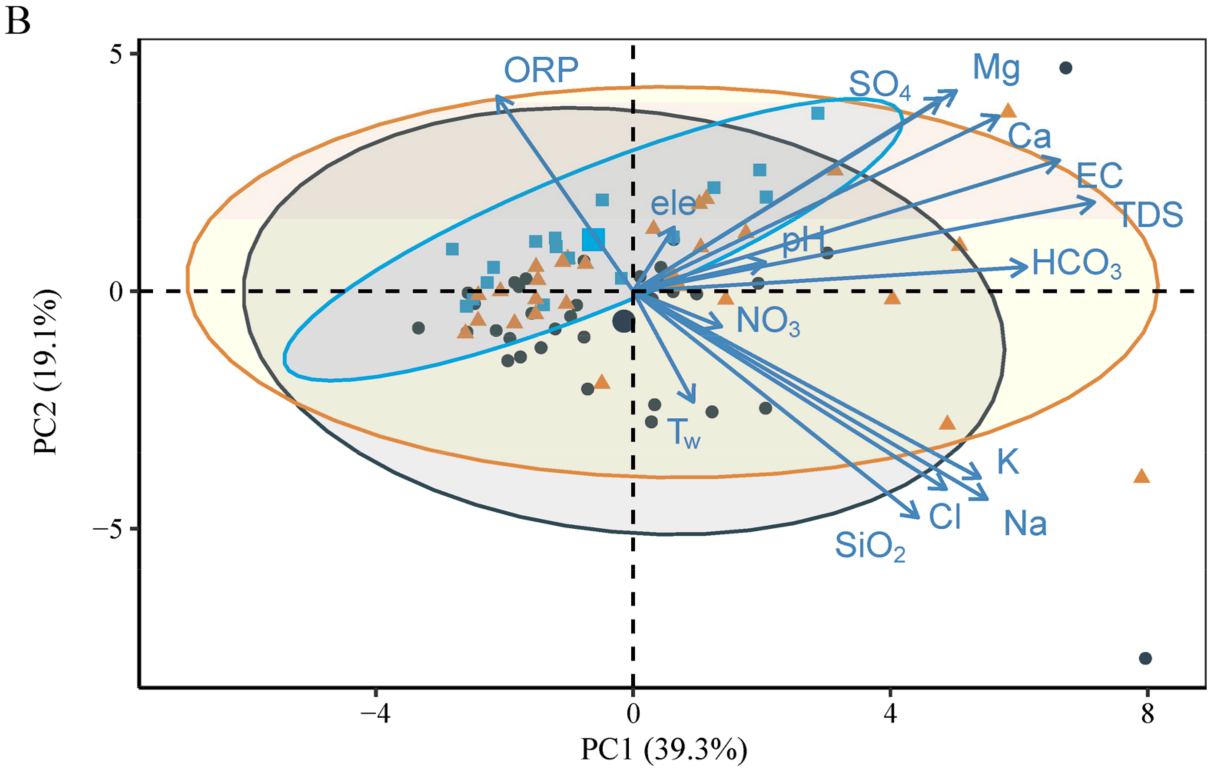

Figure 8. Biplot of the principal component analysis of the LR during the rainy season (**A**) and the dry season (**B**).

6. Conclusions

This study investigates the hydrochemical characteristics of the LR during the dry and rainy seasons. The LR water quality is relatively pristine and possesses a slightly alkaline aquatic environment with an average pH of 8.1 and a mean TDS of 165.6 ± 7.7 mg/L during the sampling period. Ca^{2+} and Mg^{2+} are the dominant cations which account for 80% of the total cations. HCO_3^- and SO_4^{2-} are the dominant anions contributing 90% of the total anions. All of the major ions show significant seasonal variations with lower concentrations in the rainy season owing to the coupled dilution of the intense precipitation and glacier meltwater. The temporal variation of NO_3^- and SO_4^{2-} is significant in both seasons. HCO_3^-, Mg^{2+}, and NO_3^- show significant spatial variations ($p < 0.05$) across the LR basin owing to the complex geological settings and anthropogenic activities.

The ternary plot, mixing diagram, and multivariate statistical analysis illustrate lithology and monsoon climate jointly drive the temporal-spatial variance of the hydrochemistry parameters. The dominant mechanism affecting the LR hydrochemistry is the parent rock weathering followed by the topography and monsoon climate as well as anthropogenic activities. NO_3^- is significantly negatively associated with elevation, which is caused by anthropogenic activities carried out in the low elevation regions. SO_4^{2-} is positively correlated with Ca^{2+}, Mg^{2+}, TDS, and EC. Geothermal springs are also an important end-member enriched in Cl^-, SO_4^{2-}, Na^+, and Ca^{2+}. The mechanisms controlling the major ions chemistry show spatial variations. Carbonate weathering is the major source of hydrochemistry in the upstream, middle stream, and downstream of the LR, respectively, followed by silicate weathering. Geothermal springs input and anthropogenic activities are also important end-members for major ions in the middle stream and downstream. There is no doubt that hydrochemistry will be under threat with the increase of anthropogenic activities, especially in the middle reaches and downstream of the LR.

Author Contributions: Conceptualization, C.Z.; methodology, M.Z.; software, M.Z.; validation, M.Z.; investigation, M.Z., Y.F., J.C. and Q.H.; resources, X.K.; data curation, M.Z., Y.H., H.Z. and Y.Z.; writing—original draft preparation, M.Z.; writing—review and editing, X.K., Y.F., Y.H., Q.H., H.Z., J.C., Y.Z. and C.Z.; visualization, M.Z.; supervision, X.K.; project administration, X.K.; funding acquisition, X.K. All authors have read and agreed to the published version of the manuscript.

Funding: This research was funded by the National Natural Science Foundation of China (Grant No. 91747204, 92047202), and High-level Special Funding of the Southern University of Science and Technology (Grant No. G02296302, G02296402).

Institutional Review Board Statement: Not applicable.

Informed Consent Statement: Not applicable.

Data Availability Statement: The data presented in this study are available on request from the corresponding author.

Conflicts of Interest: The authors declare no conflict of interest.

References

1. Vega, M.; Pardo, R.; Barrado, E.; Deban, L. Assessment of seasonal and polluting effects on the quality of river water by exploratory data analysis. *Water Res.* **1998**, *32*, 3581–3592. [CrossRef]
2. Meybeck, M.; Helmer, R. The quality of rivers from pristine stage to global pollution. *Glob. Planet. Chang.* **1989**, *75*, 283–309. [CrossRef]
3. Hren, M.T.; Chamberlain, C.P.; Hilley, G.E.; Blisniuk, P.M.; Bookhagen, B. Major ion chemistry of the Yarlung Tsangpo-Brahmaputra river: Chemical weathering, erosion, and CO_2 consumption in the southern Tibetan plateau and eastern syntaxis of the Himalaya. *Geochim. Cosmochim. Acta* **2007**, *71*, 2907–2935. [CrossRef]
4. O'Brien, A.K.; Rice, K.C.; Bricker, O.P.; Kennedy, M.M.; Anderson, R.T. Use of geochemical mass balance modelling to evaluate the role of weathering in determining stream chemistry in five mid-Atlantic watersheds on different lithologies. *Hydrol. Process.* **1997**, *11*, 719–744. [CrossRef]
5. Qu, B.; Zhang, Y.; Kang, S.; Sillanpaa, M. Water chemistry of the southern Tibetan Plateau: An assessment of the Yarlung Tsangpo river basin. *Environ. Earth Sci.* **2017**, *76*. [CrossRef]
6. Gibbs, R.J. Mechanisms controlling world water chemistry. *Science* **1970**, *170*, 1088–1090. [CrossRef]
7. Li, S.Y.; Xu, Z.F.; Wang, H.; Wang, J.H.; Zhang, Q.F. Geochemistry of the upper Han River basin, China 3: Anthropogenic inputs and chemical weathering to the dissolved load. *Chem. Geol.* **2009**, *264*, 89–95. [CrossRef]
8. Pant, R.R.; Zhang, F.; Rehman, F.U.; Wang, G.; Ye, M.; Zeng, C.; Tang, H. Spatiotemporal variations of hydrogeochemistry and its controlling factors in the Gandaki River Basin, Central Himalaya Nepal. *Sci. Total Environ.* **2018**, *622*, 770–782. [CrossRef]
9. Da Silva, A.M.M.; Sacomani, L.B. Using chemical and physical parameters to define the quality of Pardo River water (Botucatu-SP-Brazil). *Water Res.* **2001**, *35*, 1609–1616. [CrossRef]
10. Galy, A.; France-Lanord, C. Weathering processes in the Ganges-Brahmaputra basin and the riverine alkalinity budget. *Chem. Geol.* **1999**, *159*, 31–60. [CrossRef]
11. Sarin, M.M.; Krishnaswami, S.; Dilli, K.; Somayajulu, B.L.K.; Moore, W.S. Major ion chemistry of the Ganga-Brahmaputra river system: Weathering processes and fluxes to the Bay of Bengal. *Geochim. Cosmochim. Acta* **1989**, *53*, 997–1009. [CrossRef]
12. Stallard, R.F.; Edmond, J.M. Geochemistry of the Amazon 1. Precipitation chemistry and the marine contribution to the dissolved-load at the time of peak discharge. *J. Geophys. Res.* **1981**, *86*, 9844–9858. [CrossRef]
13. Huang, X.; Sillanpaa, M.; Gjessing, E.T.; Vogt, R.D. Water quality in the Tibetan Plateau: Major ions and trace elements in the headwaters of four major Asian rivers. *Sci. Total Environ.* **2009**, *407*, 6242–6254. [CrossRef] [PubMed]
14. Jiang, L.; Yao, Z.; Liu, Z.; Wang, R.; Wu, S. Hydrochemistry and its controlling factors of rivers in the source region of the Yangtze River on the Tibetan Plateau. *J. Geochem. Explor.* **2015**, *155*, 76–83. [CrossRef]
15. Huang, X.; Sillanpaa, M.; Gjessing, E.T.; Peraniemi, S.; Vogt, R.D. Water quality in the southern Tibetan Plateau: Chemical evaluation of the Yarlung Tsangpo (Brahmaputra). *River Res. Appl.* **2011**, *27*, 113–121. [CrossRef]
16. Jiang, L.; Yao, Z.; Wang, R.; Liu, Z.; Wang, L.; Wu, S. Hydrochemistry of the middle and upper reaches of the Yarlung Tsangpo River system: Weathering processes and CO_2 consumption. *Environ. Earth Sci.* **2015**, *74*, 2369–2379. [CrossRef]
17. Pritchard, H.D. Asia's shrinking glaciers protect large populations from drought stress. *Nature* **2019**, *569*, 649–654. [CrossRef]
18. Yao, T.; Xue, Y.; Chen, D.; Chen, F.; Thompson, L.; Cui, P.; Koike, T.; Lau, W.K.M.; Lettenmaier, D.; Mosbrugger, V.; et al. Recent third pole's rapid warming accompanies cryospheric melt and water cycle intensification and interactions between monsoon and environment: Multidisciplinary approach with observations, modeling, and analysis. *Bull. Am. Meteorol. Soc.* **2019**, *100*, 423–444. [CrossRef]
19. Han, P.F.; Long, D.; Han, Z.Y.; Du, M.D.; Dai, L.Y.; Hao, X.H. Improved understanding of snowmelt runoff from the headwaters of China's Yangtze River using remotely sensed snow products and hydrological modeling. *Remote Sens. Environ.* **2019**, *224*, 44–59. [CrossRef]

20. Hu, M.H.; Stallard, R.F.; Edmond, J.M. Major ion chemistry of some large Chinese rivers. *Nature* **1982**, *298*, 550–553. [CrossRef]
21. Immerzeel, W.W.; van Beek, L.P.H.; Bierkens, M.F.P. Climate change will affect the Asian Water Towers. *Science* **2010**, *328*, 1382–1385. [CrossRef]
22. Barnett, T.P.; Adam, J.C.; Lettenmaier, D.P. Potential impacts of a warming climate on water availability in snow-dominated regions. *Nature* **2005**, *438*, 303–309. [CrossRef] [PubMed]
23. Bolch, T.; Kulkarni, A.; Kaab, A.; Huggel, C.; Paul, F.; Cogley, J.G.; Frey, H.; Kargel, J.S.; Fujita, K.; Scheel, M.; et al. The state and fate of Himalayan glaciers. *Science* **2012**, *336*, 310–314. [CrossRef]
24. Lutz, A.F.; Immerzeel, W.W.; Shrestha, A.B.; Bierkens, M.F.P. Consistent increase in High Asia's runoff due to increasing glacier melt and precipitation. *Nat. Clim. Chang.* **2014**, *4*, 587–592. [CrossRef]
25. Brown, L.E.; Hannah, D.M.; Milner, A.M.; Soulsby, C.; Hodson, A.J.; Brewer, M.J. Water source dynamics in a glacierized alpine river basin (Taillon-Gabiétous, French Pyrénées). *Water Resour. Res.* **2006**, *42*, W08404. [CrossRef]
26. Li, D.; Luo, H.; Hu, T.; Shao, D.; Cui, Y.; Khan, S.; Luo, Y. Identification of the roles of climate factors, engineering construction, and agricultural practices in vegetation dynamics in the Lhasa River Basin, Tibetan Plateau. *Remote Sens.* **2020**, *12*, 1883. [CrossRef]
27. Du Laing, G.; Rinklebe, J.; Vandecasteele, B.; Meers, E.; Tack, F.M.G. Trace metal behaviour in estuarine and riverine floodplain soils and sediments: A review. *Sci. Total Environ.* **2009**, *407*, 3972–3985. [CrossRef]
28. Guo, Q.; Wang, Y.; Liu, W. Major hydrogeochernical processes in the two reservoirs of the Yangbajing geothermal field, Tibet, China. *J. Volcanol. Geotherm. Res.* **2007**, *166*, 255–268. [CrossRef]
29. Guo, Q.; Wang, Y.; Liu, W. Hydrogeochemistry and environmental impact of geothermal waters from Yangyi of Tibet, China. *J. Volcanol. Geotherm. Res.* **2009**, *180*, 9–20. [CrossRef]
30. Makokha, G.O.; Wang, L.; Zhou, J.; Li, X.; Wang, A.; Wang, G.; Kuria, D. Quantitative drought monitoring in a typical cold river basin over Tibetan Plateau: An integration of meteorological, agricultural and hydrological droughts. *J. Hydrol.* **2016**, *543*, 782–795. [CrossRef]
31. Lin, L.; Gao, M.; Liu, J.; Wang, J.; Wang, S.; Chen, X.; Liu, H. Understanding the effects of climate warming on streamflow and active groundwater storage in an alpine catchment: The upper Lhasa River. *Hydrol. Earth Syst. Sci.* **2020**, *24*, 1145–1157. [CrossRef]
32. Liu, J.; Xie, J.; Gong, T.; Wang, H.; Xie, Y. Impacts of winter warming and permafrost degradation on water variability, upper Lhasa River, Tibet. *Quat. Int.* **2011**, *244*, 178–184. [CrossRef]
33. You, Q.L.; Kang, S.C.; Wu, Y.H.; Yan, Y.P. Climate change over the Yarlung Zangbo river basin during 1961-2005. *J. Geogr. Sci.* **2007**, *17*, 409–420. [CrossRef]
34. Huang, X.; Sillanpaa, M.; Gjessing, E.T.; Peraniemi, S.; Vogt, R.D. Environmental impact of mining activities on the surface water quality in Tibet: Gyama valley. *Sci. Total Environ.* **2010**, *408*, 4177–4184. [CrossRef] [PubMed]
35. Mao, G.X.; Zhao, Y.S.; Zhang, F.R.; Liu, J.J.; Huang, X. Spatiotemporal variability of heavy metals and identification of potential source tracers in the surface water of the Lhasa River basin. *Environ. Sci. Pollut. Res.* **2019**, *26*, 7442–7452. [CrossRef] [PubMed]
36. Zhang, T.; Cai, W.; Li, Y.; Geng, T.; Zhang, Z.; Lv, Y.; Zhao, M.; Liu, J. Ion chemistry of groundwater and the possible controls within Lhasa River Basin, SW Tibetan Plateau. *Arab. J. Geosci.* **2018**, *11*, 510. [CrossRef]
37. Liu, J.; Gao, Z.; Wang, M.; Li, Y.; Shi, M.; Zhang, H.; Ma, Y. Hydrochemical characteristics and possible controls in the groundwater of the Yarlung Zangbo River Valley, China. *Environ. Earth Sci.* **2019**, *78*, 76. [CrossRef]
38. Qin, H.; Gao, B.; He, L.; Hu, X.; Dong, L.; Sanjay, D.; Dong, A.; Sun, Z.; Wan, W. Hydrogeochemical characteristics and controlling factors of the Lhasa River under the influence of anthropogenic activities. *Water* **2019**, *11*, 948. [CrossRef]
39. Li, D.; Tian, P.; Luo, H.; Hu, T.; Dong, B.; Cui, Y.; Khan, S.; Luo, Y. Impacts of land use and land cover changes on regional climate in the Lhasa River basin, Tibetan Plateau. *Sci. Total Environ.* **2020**, *742*, 140570. [CrossRef]
40. Rao, W.; Chen, X.; Meredith, K.T.; Tan, H.; Gao, M.; Liu, J. Water uptake of riparian plants in the lower Lhasa River Basin, South Tibetan Plateau using stable water isotopes. *Hydrol. Process.* **2020**, *34*, 3492–3505. [CrossRef]
41. Podila, S.P.; Penumaka, R.; Cherukuri, I. Hydrochemistry of groundwater from Chevella Watershed, Telangana State, India. *J. Geol. Soc. India* **2019**, *94*, 501–506. [CrossRef]
42. Song, C.L.; Wang, G.X.; Mao, T.X.; Huang, K.W.; Sun, X.Y.; Hu, Z.Y.; Chang, R.Y.; Chen, X.P.; Raymond, P.A. Spatiotemporal variability and sources of DIC in permafrost catchments of the Yangtze River Source Region: Insights from stable carbon isotope and water chemistry. *Water Resour. Res.* **2020**, *56*, 22. [CrossRef]
43. Alberto, W.D.; Del Pilar, D.M.; Valeria, A.M.; Fabiana, P.S.; Cecilia, H.A.; De Los Angeles, B.M. Pattern recognition techniques for the evaluation of spatial and temporal variations in water quality. A case study: Suquia River basin (Cordoba-Argentina). *Water Res.* **2001**, *35*, 2881–2894. [CrossRef]
44. Diamantini, E.; Lutz, S.R.; Mallucci, S.; Majone, B.; Merz, R.; Bellin, A. Driver detection of water quality trends in three large European river basins. *Sci. Total Environ.* **2018**, *612*, 49–62. [CrossRef] [PubMed]
45. Guggenmos, M.R.; Daughney, C.J.; Jackson, B.M.; Morgenstern, U. Regional-scale identification of groundwater-surface water interaction using hydrochemistry and multivariate statistical methods, Wairarapa Valley, New Zealand. *Hydrol. Earth Syst. Sci.* **2011**, *15*, 3383–3398. [CrossRef]
46. Singh, K.P.; Malik, A.; Mohan, D.; Sinha, S. Multivariate statistical techniques for the evaluation of spatial and temporal variations in water quality of Gomti River (India)—A case study. *Water Res.* **2004**, *38*, 3980–3992. [CrossRef]
47. Bengraine, K.; Marhaba, T.F. Using principal component analysis to monitor spatial and temporal changes in water quality. *J. Hazard. Mater.* **2003**, *100*, 179–195. [CrossRef]

48. Liu, F.; Wang, S.; Yeh, T.C.J.; Zhen, P.; Wang, L.; Shi, L. Using multivariate statistical techniques and geochemical modeling to identify factors controlling the evolution of groundwater chemistry in a typical transitional area between Taihang Mountains and North China Plain. *Hydrol. Process.* **2020**, *34*, 1888–1905. [CrossRef]
49. Nyenje, P.M.; Foppen, J.W.; Uhlenbrook, S.; Lutterodt, G. Using hydrochemical tracers to assess impacts of unsewered urban catchments on hydrochemistry and nutrients in groundwater. *Hydrol. Process.* **2014**, *28*, 5860–5878. [CrossRef]
50. Helena, B.; Pardo, R.; Vega, M.; Barrado, E.; Fernandez, J.M.; Fernandez, L. Temporal evolution of groundwater composition in an alluvial aquifer (Pisuerga River, Spain) by principal component analysis. *Water Res.* **2000**, *34*, 807–816. [CrossRef]
51. Gaillardet, J.; Dupre, B.; Louvat, P.; Allegre, C.J. Global silicate weathering and CO_2 consumption rates deduced from the chemistry of large rivers. *Chem. Geol.* **1999**, *159*, 3–30. [CrossRef]
52. Meybeck, M. Global occurrence of major elements in rivers. *Treatise Geochem.* **2003**, *5*, 207–223. [CrossRef]
53. *Chinese Standards for Drinking Water Quality*; GB 5749; Ministry of Public Health of China: Beijing, China, 2006.
54. WHO. *Guidelines for Drinking-Water Quality*; WHO Chronicle; World Health Organization: Geneva, Switzerland, 2011.
55. Singh, S.K.; Sarin, M.M.; France-Lanord, C. Chemical erosion in the eastern Himalaya: Major ion composition of the Brahmaputra and delta C-13 of dissolved inorganic carbon. *Geochim. Cosmochim. Acta* **2005**, *69*, 3573–3588. [CrossRef]
56. Blum, J.D.; Gazis, C.A.; Jacobson, A.D.; Chamberlain, C.P. Carbonate versus silicate weathering in the Raikhot watershed within the high Himalayan crystalline series. *Geology* **1998**, *26*, 411–414. [CrossRef]
57. Yang, Q.; Li, Z.; Ma, H.; Wang, L.; Martín, J.D. Identification of the hydrogeochemical processes and assessment of groundwater quality using classic integrated geochemical methods in the Southeastern part of Ordos basin, China. *Environ. Pollut.* **2016**, *218*, 879–888. [CrossRef]
58. Liu, J.; Li, Y.; Gao, Z.; Wang, M.; Liu, M.; Wang, S.; Wang, Z. Hydrochemistry and relationship between groundwater and surface water in the middle and lower reaches of Lhasa River basin. *J. Shandong Univ. Sci. Technol. Nat. Sci.* **2020**, *39*, 10–20, (In Chinese with English abstract).
59. Quade, J.; English, N.; DeCelles, P.G. Silicate versus carbonate weathering in the Himalaya: A comparison of the Arun and Seti River watersheds. *Chem. Geol.* **2003**, *202*, 275–296. [CrossRef]
60. Tsering, T.; Abdel Wahed, M.S.M.; Iftekhar, S.; Sillanpää, M. Major ion chemistry of the Teesta River in Sikkim Himalaya, India: Chemical weathering and assessment of water quality. *J. Hydrol. Reg. Stud.* **2019**, *24*, 100612. [CrossRef]
61. Zhao, P.; Ji, D.; Jian, J. A new geochemical model of the Yangbajing geothermal field, Tibet. Proceedings World Geothermal Congress, Kyushu-Tohoku, Japan, 28 May–10 June 2000; pp. 2007–2012.